GEOPHYSICS, VOL. 73, NO. 6 (NOVEMBER-DECEMBER 2008); P. F223–F234, 11 FIGS., 1 TABLE.
10.1190/1.2987375

Robust processing of magnetotelluric data in the AMT dead band using the continuous wavelet transform

Xavier Garcia[1] and Alan G. Jones[2]

ABSTRACT

The energy sources for magnetotellurics (MT) at frequencies above 8 Hz are electromagnetic waves generated by distant lightning storms propagating globally within the earth-ionosphere waveguide. The nature of the sources and properties of this waveguide display diurnal and seasonal variations that can cause significant signal amplitude attenuation, especially at 1–5 kHz frequencies — the so-called audiomagnetotelluric (AMT) dead band. This lack of energy results in unreliable MT response estimates; and, given that in crystalline environments ore bodies located at some 500–1000-m depth are sensed initially by AMT data within the dead band, this leads to poor inherent geometric resolution of target structures. We propose a new time-series processing technique that uses localization properties of the wavelet transform to select the most energetic events. Subsequently, two coherence thresholds and a series of robust weights are implemented to obtain the most reliable MT response estimates. Finally, errors are estimated using a nonparametric jackknife algorithm. We applied this algorithm to AMT data collected in northern Canada. These data were processed previously using traditional robust algorithms and using a telluric-telluric magnetotelluric (TTMT) technique. The results show a significant improvement in estimates for the AMT dead band and permit their quantitative interpretation.

INTRODUCTION

Time-varying, natural-source electromagnetic (EM) waves observable on the earth's surface at frequencies above about 8 Hz are generated by distant lightning activity and, at frequencies below 8 Hz, by the interaction of the earth's magnetosphere with particles ejected by the sun (solar plasma). The former are important for audiomagnetotelluric (AMT) studies of upper crustal structures for environmental, energy, and resource exploration purposes, such as groundwater contamination, geothermal exploration, and discovery of economic mineralization. Lightning-induced waves propagate around the globe in the electrically charged earth-ionosphere waveguide (Thomson, 1860; Wilson, 1920), and they penetrate the earth and respond in amplitude and phase to the subsurface electrical conductivity structure.

Properties of the waveguide and the frequency characteristics of lightning display diurnal and seasonal variations that can cause significant signal amplitude variations, especially in the 1–5 kHz so-called AMT dead band. These variations show an increase in amplitude during the summer months in the northern hemisphere and at nighttime, and a corresponding decrease during the winter months and daytime. Thus, one problem associated with applying the AMT method for shallow (<3km) exploration can be the lack of signal in certain frequency bands during the desired acquisition interval. For more information on AMT source analysis, see Garcia and Jones (2002).

Traditional processing of MT data was based on approximations of the least-squares method and assumptions of an ergodic, Gaussian statistical model (Bendat and Piersol, 1971; Sims et al., 1971), and both are sensitive to small amounts of anomalous data and uncorrelated noise. The inadequacy of the statistical model can cause the magnetotelluric (MT) tensor to be strongly biased and unusable. These biases were discussed first in MT by Sims et al. (1971); but they were known in other fields much earlier, particularly in econometrics (Gini, 1921), and were discussed in Reiersøl (1950). The remote reference (RR) method (Gamble et al., 1979) was developed to introduce bias control in MT data processing.

The first use of such an unbiased estimator for transfer function estimation again comes from econometrics (Reiersøl, 1941), and independently from Geary (1943); see Reiersøl (1950) and Akaike (1967), in which remote reference fields were termed instrumental variables. The RR method consists of simultaneous recording (typically) the horizontal magnetic fields measured at a second site that is

Manuscript received by the Editor 27 July 2007; revised manuscript received 5 April 2008; published online 5 November 2008.
[1]Formerly Dublin Institute for Advanced Studies, Dublin, Ireland; presently Institut de Ciéncies del Mar, CSIC, Barcelona, Spain. E-mail: xgarcia@icm.csic.es.
[2]Dublin Institute for Advanced Studies, Dublin, Ireland. E-mail: alan@cp.dias.ie.

sufficiently remote from the main site so that noise sources are uncorrelated between the sites. Given the correct assumption that noise sources at both locations are uncorrelated, this method is effective in removing the bias caused by uncorrelated noise. However, there exist unusual noise sources (complex natural sources or cultural noise) and frequency bands (MT and AMT dead bands), which can cause the RR method to fail.

Coherence-sorting methods also have been applied. Data from low signal-to-noise-ratio frequency bands (e.g., MT or AMT dead bands) have been treated with a presorting method to eliminate low coherence segments (Egbert and Livelybrooks, 1996; Smirnov, 2003), although the method is not always useful (Chave and Jones, 1997).

The introduction of data-adaptive weighting schemes, sometimes along with the RR method, have been shown to eliminate the influence of outliers in electric fields (Jones and Joedicke, 1984; Egbert and Booker, 1986; Chave et al., 1987; Chave and Thomson, 1989; Larsen, 1989). Jones et al. (1989), who compare different MT processing schemes applied to the same data set, document the superiority of these robust processing methods. Schultz et al. (1993) interpreted the contamination of data collected using a large electrode array (>1km spans), with electrodes at the bottom of a large lake (Carty Lake) in northern Ontario, Canada, as the result of aurora (Northern Lights). This interpretation led to the development of a robust processing technique with a leverage control that could detect contaminated data in electric and magnetic fields. More recently, Egbert and Livelybrooks (1996) and Chave and Thomson (2003, 2004) extended the removal of outliers to the magnetic fields.

Finally, Trad and Travassos (2000) introduce an approach using the wavelet transform. These authors use the discrete wavelet transform (DWT). A series of robust weights were applied to the transformed data to remove noise. Subsequently, a robust processing technique was applied to the antitransformed filtered data.

Another key component of processing, which indeed is as important as estimation of the response functions themselves, is the calculation of their confidence limits. Least-squares impedance errors based on Gaussian distributions typically are biased (Chave and Jones, 1997) and unable to provide reliable uncertainty estimates. In comparison, nonparametric methods are distribution independent; and thus the error estimates are more accurate. The nonparametric jackknife method of Richard von Mises (see Efron, 1982) for error estimation was introduced to MT processing by Chave and Thomson (1989) and subsequently justified rigorously (Thomson and Chave, 1991).

These estimation techniques, initially developed for processing long-period MT data, also have been applied to process AMT data. As mentioned previously, because of source characteristics the issues related to problems in the AMT frequency band differ from those in the MT band; and these codes can fail to provide reliable estimates of AMT transfer functions at frequencies of 1 kHz through 5 kHz. In particular, at high latitudes often there is little observable signal; and the few transients that are recorded must be located perfectly in the time series, otherwise, the codes fail (Garcia and Jones, 2002). Garcia and Jones (2005) introduce a new methodology based on the use of electric transfer functions between sites and a base station, and on robust MT transfer functions from the base station recorded at night, to solve the problem of lack of energy in the AMT dead band at high latitudes.

For nonperiodic, nonstationary time series, the Fourier transform can give spurious results that have been solved to some extent with the introduction of windowed Fourier transforms. As an alternative approach, the wavelet transform might have advantages compared with the Fourier transform for spectral analysis. Zhang and Paulson (1997) were the first to use wavelets, in their case the continuous wavelet transform (CWT), for processing AMT data. In their work, the CWT is used to localize high-energy events. Then a new coherence thresholding technique, defined by the authors, permitted isolating bad data points.

This new coherence function assumes that the diagonal components of the impedance tensor are almost zero compared with the off-diagonal elements (Zhang et al., 1997). For this reason, this technique can fail in the presence of complicated three-dimensional geology or galvanic distortions (McNeice and Jones, 2001). The use of a standard least-squares method to obtain the transfer functions also makes this technique sensitive to the presence of strong noise. Nevertheless, the CWT has good localization properties.

In this paper, we extend the work of Zhang and Paulson (1997) that uses the CWT as a means to obtain spectra of the time series. After calculating the wavelet spectra, the magnetic spectra are analyzed to locate the high-energy events. These can be either signal or noise, and for this reason we apply a coherence threshold method and a robust weighting technique to eliminate segments contaminated by uncorrelated noise. This method is completed with the use of a jackknife nonparametric error-estimate technique for the calculation of confidence levels.

WAVELET TRANSFORM

In this section, we briefly describe the method of wavelet analysis. General bibliography on wavelets can be found in Daubechies (1990), Mallat (1998), and Percival and Walden (2000). A description of the wavelet transform as applied to geophysics can be found in Foufoula-Georgiou and Kumar (1995), and details about the applicability of wavelet analysis can be found in Weng and Lau (1994), Meyers et al. (1993), and Torrence and Compo (1998).

To analyze signal structures of very different sizes, it is necessary to use time-frequency functions called atoms with varying time supports (an example of an atom would be the taper window used to calculate the Fourier transform). The wavelet transform (WT) is capable of providing the time and frequency information simultaneously, hence giving a time-frequency representation of the signal. The wavelet transform is based on the two-parameter family of dilated and translated functions. Decomposing signals over this family of functions can be used to analyze time series that contain nonstationary power at many different frequencies (Daubechies, 1990).

Let $\psi(t)$ be a fixed function (mother wavelet), and consider a two-parameter family of dilated and translated functions; thus

$$\psi_{b,s} = \frac{1}{s}\psi\left(\frac{t-b}{s}\right), \tag{1}$$

where s and b are the scale and translation parameters, respectively. Functions in the family obtained from equation 1 also are known as daughter functions. The term translation is used in the same sense as

in the windowed Fourier transform: It is related to the location of the window as the window is shifted through the signal. This term obviously corresponds to time information in the transform domain. However, we do not have a frequency parameter, as we had for the Fourier transform. Instead, we have a scale parameter that is related to the inverse of the frequency.

To be admissible as a wavelet, a function must satisfy certain mathematical criteria. First, a wavelet must have finite energy;

$$E = \int_{-\infty}^{\infty} |\psi(t)|^2 dt < \infty, \tag{2}$$

where E is the energy of a function equal to the integral of its squared magnitude, and the vertical brackets ‖ represent the magnitude operator of ψ. If $\psi(t)$ is a complex function, the magnitude must be found using its real and imaginary parts.

Second, considering $\hat{\psi}(f)$ as the Fourier transform of $\psi(t)$, the following condition must hold:

$$C_g = \int_0^{\infty} \frac{|\hat{\psi}(f)|^2}{f} df < \infty. \tag{3}$$

This implies that the wavelet has no zero-frequency component, $\hat{\psi}(0) = 0$; or, which is the same, the wavelet $\psi(t)$ must have a zero mean. Equation 3 is known as the admissibility condition (Farge, 1992), and C_g is called the admissibility constant. A third criterion that applies to complex wavelets is that the Fourier transform of the mother wavelet must be real and vanish for negative frequencies.

Given a time series, x_n, with a time spacing δt and $n = 0,\ldots,N-1$, the wavelet transform of x with respect to ψ is defined as

$$\mathcal{W}_g x(b,s) = \langle \psi_{b,s} | x \rangle = \int_{-\infty}^{+\infty} dt \frac{1}{s} \psi^* \left(\frac{t-b}{s} \right) x(t), \tag{4}$$

$$b \in \Re, \quad s > 0,$$

where $(*)$ indicates the complex conjugate. The continuous wavelet transform of a discrete sequence x_n similarly is defined as the convolution of x_n with a discrete scaled and translated version of the mother wavelet $\psi_0(h)$; thus

$$W_n(s) = \sum_{n'=0}^{N-1} x_n \cdot \psi^* \left[\frac{(n'-n)\delta t}{s} \right]. \tag{5}$$

Equation 5 measures the variation of x in the neighborhood of n, whose size is proportional to s. Mallat (1998, chap. 6) proves that when the scale s goes to zero, the decay of the wavelet coefficients characterizes the regularity of x close to n; in other words, the lower the scale, the more localized the information that is obtained.

According to equation 5, to calculate the WT of a time series of length N requires N convolutions. Given that in the Fourier domain the N convolutions can be done simultaneously, the discrete Fourier transform (DFT) can be employed to speed up calculation of the CWT (Kaiser, 1994). The DFT of time series x_n can be defined as

$$\hat{x}_k = \frac{1}{N} \sum_{n=0}^{N-1} x_n e^{-2\pi i k n/N}, \tag{6}$$

where $k = 0,\ldots,N-1$ is the frequency index.

Applying the convolution theorem, the wavelet transform (equation 5) can be rewritten as the inverse Fourier transform of the product, or

$$W_n(s) = \sum_{k=0}^{N-1} x_k \hat{\psi}^*(s\omega_k) e^{i\omega_k n \delta t}, \tag{7}$$

where the angular frequency ω_k is defined as

$$\omega_k = \begin{cases} \dfrac{2\pi k}{N\delta t}, & k \le \dfrac{N}{2}, \\ -\dfrac{2\pi k}{N\delta t}, & k > \dfrac{N}{2}. \end{cases} \tag{8}$$

Using equation 7 and a standard Fourier transform routine, the CWT can be calculated (for a given scale s) at all n data points simultaneously and efficiently.

Because we are dealing with finite time series and using a Fourier transform that assumes these are cyclic, we have edge effects at the beginning and end of the wavelet power spectrum. The cone of influence (COI) is the region of the wavelet spectrum in which edge effects become important. In this work, we have followed the definition of the COI by Torrence and Compo (1998) as the e-folding time for the autocorrelation of wavelet power at each scale. The COI also defines at each scale the decorrelation time for a single spike in the time series.

The algorithm that we have developed accepts a choice of two mother wavelets, either the Morlet or the Paul (Torrence and Compo, 1998) wavelet. The one that we have found most successful in our work is the Morlet wavelet (Figure 1), and we restrict discussion in this section to this type of function. The Morlet wavelet was introduced for geophysical exploration by Goupillaud et al. (1984); it consists of a plane wave localized by a Gaussian function (Grossman and Morlet, 1987). Thus

$$\psi_0(s) = \pi^{1/4} e^{i\omega_0 \eta} e^{-s^2/2}, \tag{9}$$

where ω_0 is the nondimensional frequency, in our work equal to $\pi\sqrt{2/\log(2)}$.

Strictly speaking, the Morlet wavelet, equation 9, is not a wavelet because the admissibility condition, equation 3, does not hold. However, if $\omega_0 > 0$ is large enough; or, which is the same, if the scale s is large enough, the negative frequency components of ψ are small compared with the progressive component (Mallat, 1998); and this

satisfies the admissibility condition. The parameter ω_0 allows tradeoff between time and frequency resolutions. The particular choice of ω_0 in this work avoids problems with the Morlet wavelet at low scales (high temporal resolution), at the same time that it optimizes localization properties of the wavelet in the temporal and spectral domains. Smaller values will improve the temporary localization properties while worsening the frequency localization, whereas larger values will emphasize the localization in the frequency domain.

The relationship between the equivalent Fourier period and the wavelet scale can be derived analytically for a particular wavelet function transforming a cosine wave of a known frequency, and computing the scale s at which the wavelet power spectrum reaches its maximum (Torrence and Compo, 1998). For the Morlet wavelet, the Fourier period is expressed as

$$T = \frac{4\pi s}{\omega_0 + \sqrt{2 + \omega_0}}. \quad (10)$$

Using equation 7, by varying the wavelet scale s and translating along the localized time index n, one can construct an image showing the amplitude of any features versus the scale and how this amplitude varies with time. We used this fact to localize high-energy events better in the time series. To see the relationship between the wavelet and Fourier spectra, the global wavelet spectrum must be introduced. This is defined as the average of the wavelet spectra over scales,

$$\bar{W}^2(s) = \frac{1}{N}\sum_{n=0}^{N-1} |W_n(s)|^2. \quad (11)$$

When smoothed, the Fourier spectrum approaches the global wavelet spectrum. Percival (1995) shows that the global wavelet spectrum (equation 11) provides an unbiased and consistent estimator of the true power spectrum of a time series.

Figure 2 shows 1024 points (~0.025 s) of an electric field (east-west component) and the corresponding magnetic field (north-south component) of some time series analyzed herein. This particular segment displays the arrival of a magnetotelluric transient caused by distant lightning. Figure 3 shows the wavelet spectrum for the time series in Figure 2. As can be observed, the spectrum has minimal power in the AMT dead band. The arrival of a transient caused by distant lightning enhances the energy in the AMT dead band, although it still displays a minimum centered at 2000 Hz for the magnetic field.

Localizing high-energy events can be the key to obtaining good estimates in the dead-band, although there are two problems. One problem is caused by lack of signal, even in presence of a transient; the other is caused by the presence of noise. To overcome the problem with noise, we propose the use of a robust remote reference technique to downweight those noisy segments and allow for a selection of clean high-energy events.

ROBUST PROCESSING

Jones and Joedicke (1984) propose a heuristic, jackknife robust processing method for MT data, based on maximizing coherence. This method later was modified to minimize variance and extended for multiple remote references (method 6 in Jones et al., 1989). Egbert and Booker (1986) and Chave and Thomson (1989) introduced formal, M-regression robust processing methods in MT. Chave and Thomson (2004) extend the methods to allow for several reference sites. In this work, we consider a single reference site. The following section focuses on the use of robust methods with one remote reference site.

After the time series have been transformed into the time/frequency domain, the next step is to calculate the transfer functions. In the absence of noise, the fundamental MT equation (Dmitriev and Berdichevsky, 1979) can be expressed as

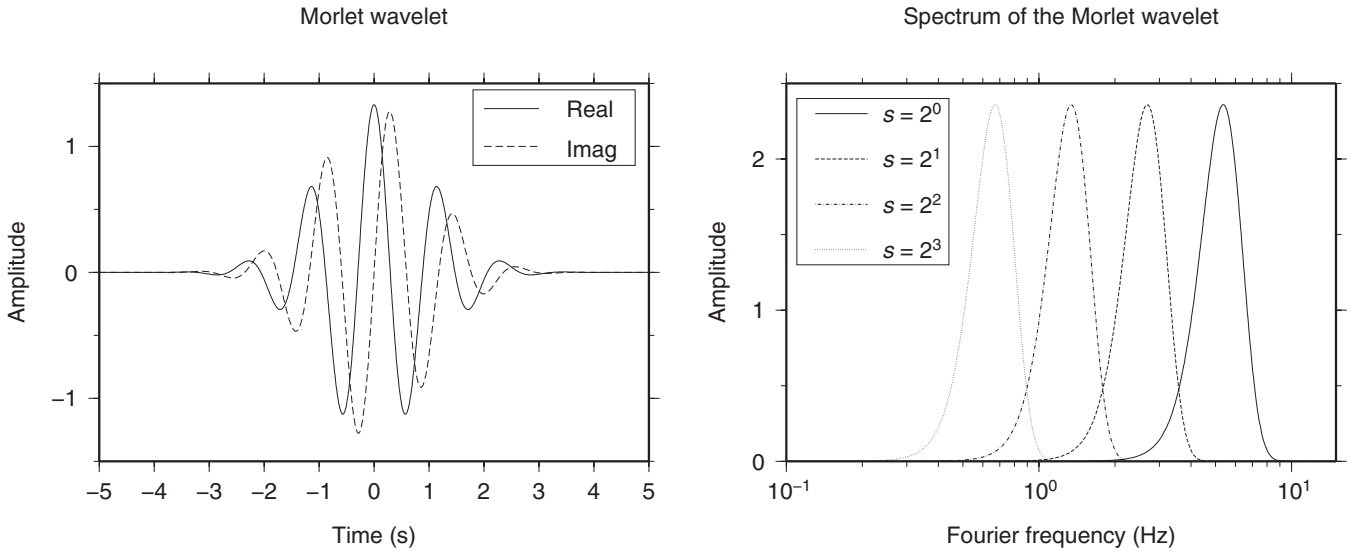

Figure 1. Morlet wavelet. Left: Time representation of the Morlet mother wavelet for a time parameter $\omega_0 = \pi\sqrt{2/\log(2)}$. Right: Fourier spectrum of the mother wavelet for four dilations (see legend). Note that each spectrum has been scaled down by its corresponding scale factor.

$$\mathbf{e} = \mathbf{zb}, \tag{12}$$

where **e** and **b** are two vectors containing the spectra of variations of the electric and magnetic fields, respectively; and **z** is a 2×2 impedance tensor. To solve this equation when the error distribution is not normal, particularly when the errors are long-tailed, the robust regression can be employed (Box, 1953). In general, a robust statistical estimator is the one that is insensitive to small departures from idealized assumptions for which the estimator is optimized (Jones et al., 1989).

The most common general method of robust regression is the M-estimation, introduced by Huber (1964). This method uses the following linear model of equation 12,

$$\mathbf{e}_i = \mathbf{b}_i\mathbf{z} + \varepsilon_i, \tag{13}$$

where ε denote the residuals, and i is the sample number. Robust procedures minimize an objective or loss function that is a function of the residuals. The robust procedure that we have used in this work uses a weighted least-squares method that minimizes $\Sigma\,\omega_i^2\varepsilon_i^2$ (Egbert and Booker, 1986; Chave and Thomson, 2004), where ω represents the robust weights.

However, the solution to this system of equations is not trivial, because the weights depend upon the residuals; the residuals depend upon the estimated coefficients; and the estimated coefficients depend upon the weights. An iterative solution (called iteratively reweighted least-squares, or IWLS) therefore is required:

1) Select initial estimates $\mathbf{z}^{(0)}$, such as the least-squares estimates.
2) At each iteration t, calculate residuals $\varepsilon_i^{(t-1)}$ and associated weights $\omega_i^{(t-1)} = \omega[\varepsilon_i^{(t-1)}]$ from the previous iteration.
3) Solve for the new weighted least-squares estimates using the following equation, which is a generalized solution to the general least squares for equation 13,

$$\mathbf{z}^{(t)} = [\mathbf{b}^{\mathbf{H}}\mathbf{w}^{(t-1)}\mathbf{b}]^{-1}\mathbf{b}^{\mathbf{H}}\mathbf{w}^{(t-1)}\mathbf{e}, \tag{14}$$

where **b** is the model matrix corresponding to the input channel, with $\mathbf{b}^{\mathbf{H}}$ as its conjugate Hermitian; and $\mathbf{w}^{(t-1)} = \mathbf{diag}\{\omega_i^{(t-1)}\}$ is the current weights matrix.

Steps 2 and 3 are repeated until the variances of the residuals converge. The convergence is defined either by not improving its value or by obtaining a change in it between iterations below a threshold value.

The procedure followed in this work is described with more detail in Chave and Thomson (1989, 2003, 2004). It consists of initially performing a few iterations using the Huber estimator as objective or

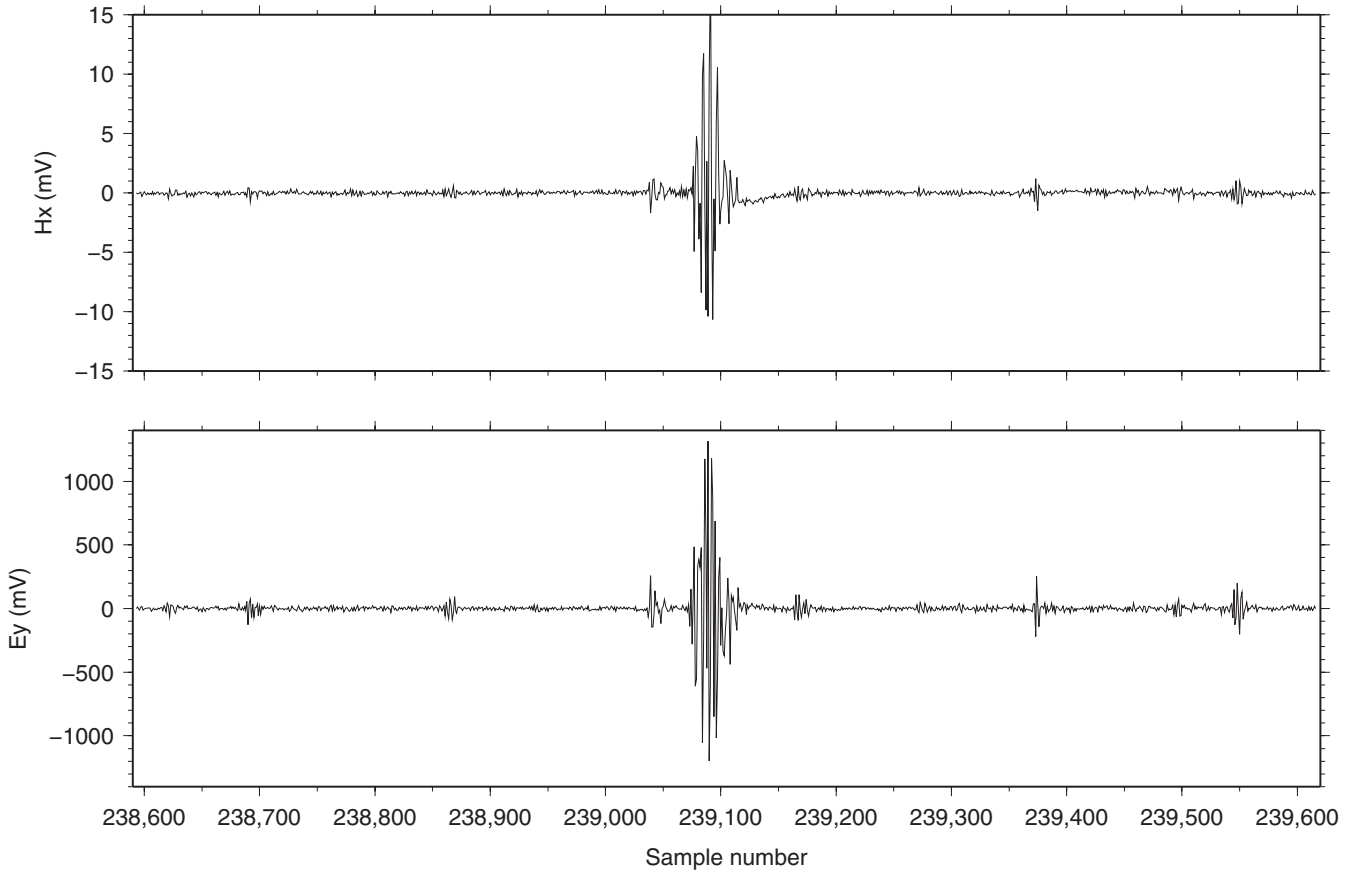

Figure 2. Example of the time series used in this work (site 001). Top: Magnetic field (Hx) recorded with an azimuth of −25°. Bottom: Electric field (Ey) recorded with an azimuth of 65°. These two time series display a transient caused by distant lightning. The abscissa shows the sample number. In this case, it covers 1024 points, equivalent to 25 ms. Note that the system response has not been corrected from these time series. They are shown here for visualization purposes.

loss function. Then, using the more severe Thomson estimator, more data are downweighted. Depending on data quality, this procedure takes only between three and eight iterations for each objective function.

The remote reference method uses electromagnetic fields acquired at a distant location to minimize the local variance of the residuals. Following Chave and Thomson (1989), the weighted least-squares solution equivalent to equation 14 for a single remote reference can be written

$$\mathbf{z}^{(t)} = [\mathbf{f}_{\mathbf{R}}^{\mathbf{H}}\mathbf{w}^{(t-1)}\mathbf{b}]^{-1}\mathbf{f}_{\mathbf{R}}^{\mathbf{H}}\mathbf{w}^{(t-1)}\mathbf{e}, \tag{15}$$

where $\mathbf{f}_{\mathbf{R}}$ is the remote field used as a reference. The robust procedure for the remote reference case is the same as the one described in this section. A more general form of the IWLS (equation 14) can be found in Chave and Thomson (2004); it includes the use of several references sites.

When the mean and variance of a set of independent and identically distributed data in the time domain are known, it is a simple task to infer estimates of standard errors. However, it is common that data sets have mixed or very complicated (e.g., multivariate) error distributions; there are outliers, or an unknown number of degrees of freedom caused by correlation and heteroscedasticity. In such cases, nonparametric methods are more appropriate to estimate the bias and standard error in a statistic when a random sample of observations is used to calculate it.

In this work, we have used the jackknife method to calculate the confidence levels of the responses. The basic idea underpinning the jackknife estimator lies in systematically recomputing the statistic estimate leaving out one observation at a time from the sample (so-called delete-one estimates). From this new set of observations for the statistic, an estimate for the bias and an estimate for the variance of the statistic can be calculated (Thomson and Chave, 1991).

Thomson and Chave (1991), among others, studied in detail the application of the jackknife method to the regression problem. To solve the linear equation 14, a new set of pseudovalues can be used (Hinkley, 1977), so that

$$\tilde{z}_i = \hat{z} - N(1 - h_i)(\hat{z} - \hat{z}_{\hat{i}}), \tag{16}$$

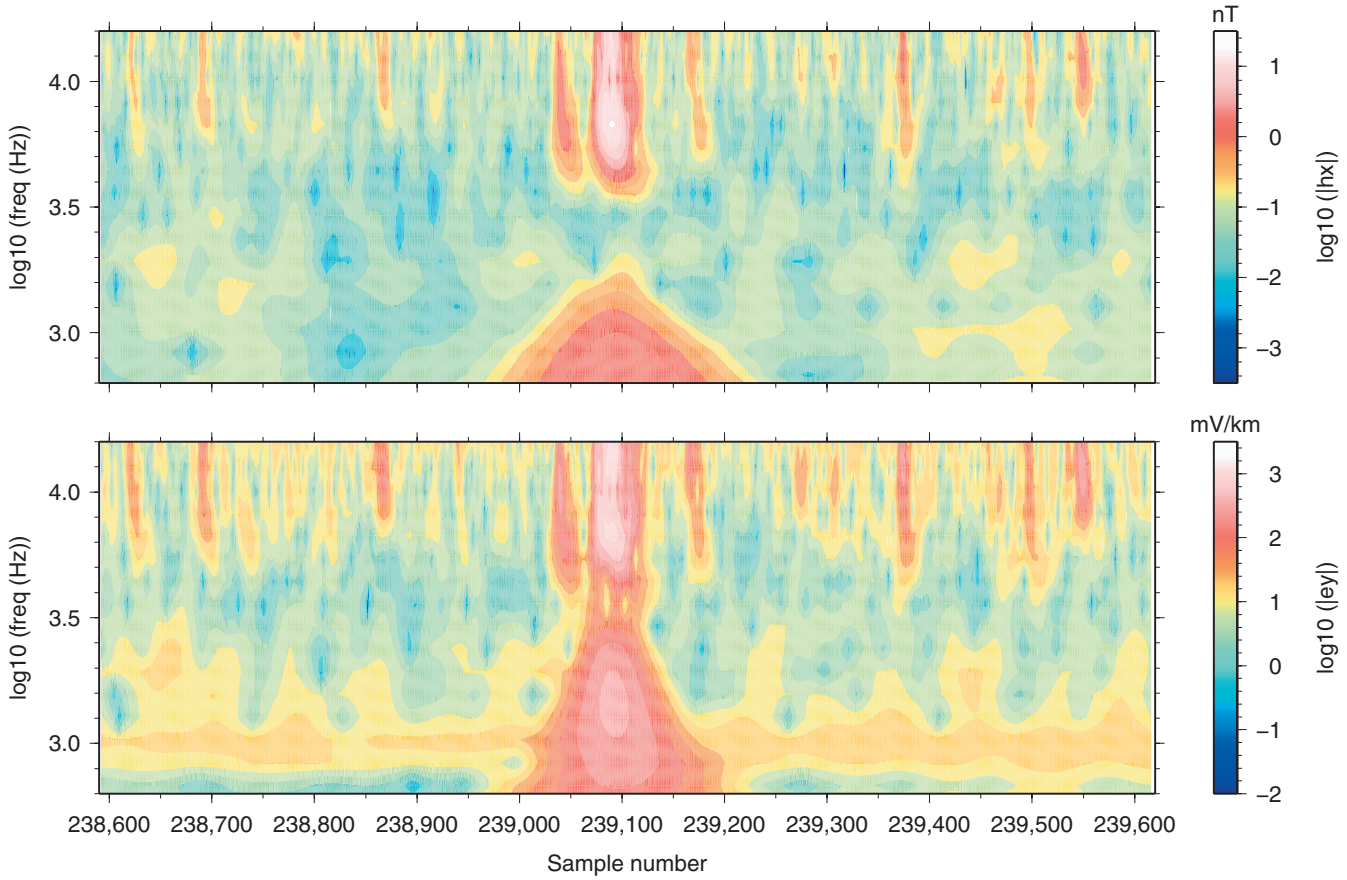

Figure 3. Morlet wavelet transform of the time series used in Figure 2. These plots show the spectral and temporal structure of the transient. It can be seen that despite the arrival of a transient, the energy levels in the dead band (1–5 kHz) remain low. Note that the system response has been corrected in the spectra.

where $\tilde{z}$ is the jackknifed estimate of the impedance $\mathbf{z}$; $\hat{z}$ is an estimate of the impedance; $\hat{z}_i$ is the estimate of the impedance based of the ith subset (the subset with the ith observation deleted); and h_i is the ith element of the diagonal of the hat matrix.

The hat matrix is a projection matrix from $\mathbf{e}$ into the column space of $\mathbf{z}$, defined as

$$\mathbf{H} = \mathbf{b}(\mathbf{b}^H\mathbf{b})^{-1}\mathbf{b}^H, \tag{17}$$

where the superscript H denotes the Hermitian conjugate. Finally, the variance estimate of the impedance $\mathbf{z}$ can be determined using

$$\text{var}\{\hat{z}\} = \frac{1}{N(N-p)}\sum_{i=1}^{N}(\tilde{z}_i - \hat{z})(\tilde{z}_i - \hat{z})^H, \tag{18}$$

where p is the number of columns in $\mathbf{z}$.

Diagonal elements of the hat matrix measure the distance of single model points from the center of the model, and the lack of balance is reflected in their size. This allows for control of the leverage or influence that elements of $\mathbf{b}$ have in the final estimate of $\mathbf{z}$ (Chave and Thomson, 2003).

ROBUST WAVELET PROCESSING ALGORITHM

The previous two sections briefly described the background information on the procedure followed in this work. The algorithm we have designed calculates wavelet spectra of the electric and magnetic time series recorded at a site, and the reference fields recorded at a remote site. From those spectra, we derive MT response function estimates using robust methods.

The reason for choosing a particular wavelet has to do with the type of problem to be explored. In magnetotellurics, the spectra are calculated to obtain the transfer functions; thus a complex, nonorthogonal wavelet is appropriate. As the electromagnetic spectra are smoothly varying with frequency, the use of smooth, undulating wavelets is appropriate. The current algorithm allows use of two mother wavelets, either the Morlet or the Paul. In our experience, the Morlet wavelet is better suited for magnetotellurics because it offers a better trade-off between time and frequency resolution, whereas the Paul wavelet has better localization properties in the time domain.

After the wavelet spectra have been derived, the ensemble then is purged of those segments for which the amplitude spectra are about the noise level of the magnetometers. This value can be set to the value provided by the instrument manufacturer. It has been shown (Garcia and Jones, 2002) that in severe quiet times in the AMT dead band, the data recorded by the magnetometers correspond to their noise levels. In addition, those segments located outside the COI of the wavelet transform are purged also. To avoid rejecting too many segments, and because computer memory is no longer an issue, we usually calculate the CWT of the whole time series; the alternative is to chop them into smaller sections, saving memory but sacrificing segments at the edges.

The next stage consists of the application of a series of coherence filters to the spectra, which permits detection of uncorrelated sections. Two kinds of coherence functions are used, a classical coherence and a wavelet coherence. The classical thresholding technique that is applied initially to the spectra uses the auto and cross-spectra of the EM time series and can be defined as

$$\gamma^2 = \frac{|\langle W^{ab}\rangle|^2}{\langle W^{aa}\rangle\langle W^{bb}\rangle}, \tag{19}$$

where $\langle\cdot\rangle$ indicates smoothing in time. Those sections in which coherence is below a specific threshold defined by the user are discarded.

A wavelet coherence technique (Torrence and Webster, 1999) is applied. Whereas the classical coherence technique searches for coherent segments along the temporal axis, the wavelet coherence function allows for a search for noncoherent segments across scales and time axes. The wavelet squared coherence function is defined as

$$\gamma^2_{\text{wavelet}} = \frac{|\langle s^{-1}W^{ab}\rangle|^2}{\langle s^{-1}|W^{aa}|^2\rangle\langle s^{-1}|W^{bb}|^2\rangle}, \tag{20}$$

where $\langle\cdot\rangle$ indicates smoothing in both time and scale. The factor s^{-1} is used to convert to an energy density.

In general, low and high power segments are rejected, because they are susceptible to either not being coherent or being strongly affected (overwhelmed) by coherent noise. Lower and upper values for the threshold can be set in the algorithm. In some instances, noise can be correlated severely between the channels; and the upper thresholding permits eliminating some of this noise. This method should be used with care because it also can eliminate clean sections. The remaining segments are used for the final response calculation. At this point, the responses are calculated and will be used as a starting estimate for the robust processing and as nonrobust estimates.

The next step consists of calculation of the hat matrix for later use in the jackknife calculation of confidence intervals. The hat matrix is used in statistics to identify high leverage points that are outliers among the independent variables. The algorithm that we have designed allows one to set a thresholding level based on the diagonal of the hat matrix, although the tests that we have run suggest no improvement of the final responses. After this step, the robust iteration process step is initiated, and it downweights the remaining noisy segments. The final stage involves calculation of the confidence levels using a jackknife procedure.

The algorithm is written in standard FORTRAN 95. Each of the time series used in this work consists of 262,144 points with a sample rate of 40,960 Hz (6.4 s in total time length); the total processing time is about two minutes on a Pentium PC.

EXAMPLE: THE NORMAN TOWNSHIP DATA SET

We applied the robust code that we present here to data acquired in July 2000 in Norman Township (Sudbury, Ontario, Canada). This experiment was designed to test a new telluric-telluric magnetotellu-

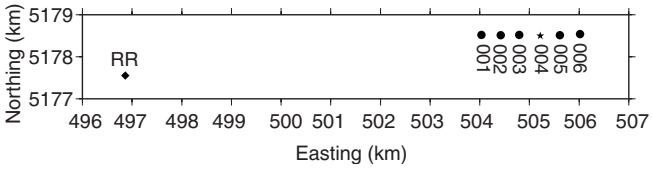

Figure 4. Location of the northern profile with sites used in this work from Norman Township experiment that tested a new (TTMT) methodology to acquire and process data to improve responses in the AMT dead band. The site marked with a diamond indicates the location of the remote reference site (Garcia and Jones, 2005). This area is located in UTM (WGS84, zone 17).

Table 1. Table showing site occupancy (GMT-5:00 EST) for sites used on July 20, 2000.

Site name occupancy (local time, GMT-5:00 EST)						
RR	001	002	003	004	005	006
11:40	11:40					
13:00		13:00		13:00		
14:00			14:00			
15:40					15:40	
				16:40		16:40

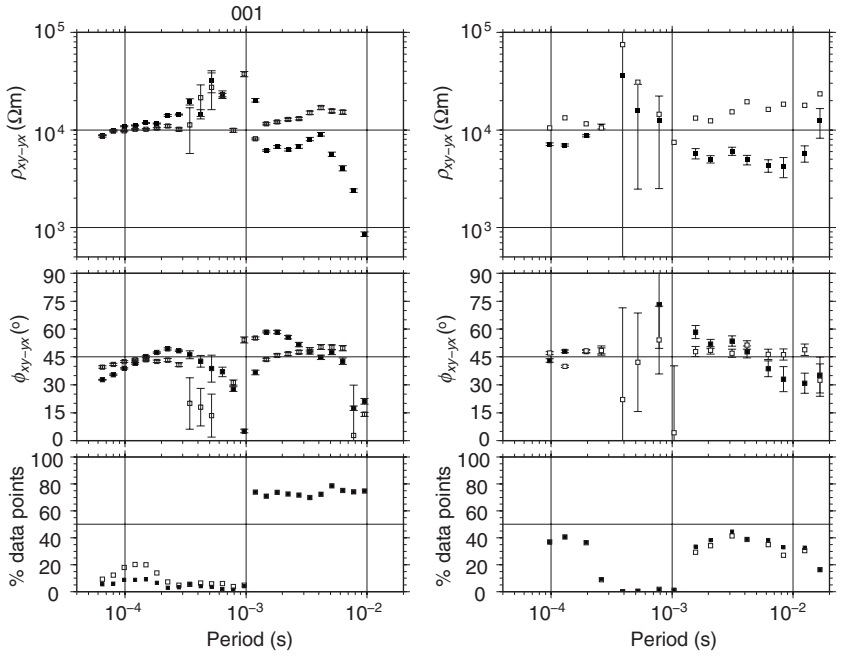

Figure 5. Apparent resistivities and phases at site 001 computed using CWT (left) and BIRRP (right) methods. Black symbols correspond to the *zxy* impedances and white symbols to the *zyx* impedances. On the bottom panel is a plot of the percentage of data remaining after rejection by coherence thresholding.

ric methodology (TTMT) proposed by Garcia and Jones (2005), and involved acquiring four profiles of AMT data with a remote reference site. The TTMT method consists of the use of electric-field daytime measurements at all stations (profile, base, and remote), and nighttime measurements at the base and remote stations. Using the transfer functions between daytime and nighttime time series, a TTMT response function can be calculated for measurements acquired during daytime.

In this work, we process data from the northern profile of the survey (Figure 4), and compare the resulting estimates with previous best estimates from robust, conventional MT processing. Because the experiment was designed to test the TTMT method, data were acquired at different times of the day. Table 1 summarizes site occupancy of data recorded on July 20, 2000. Unfortunately, for site 006 the remote reference was not recording. We have used the only site available at that time, 004, as a reference.

Processing consists of four fundamental steps. First, time series are transformed into the spectral domain using wavelet methods. Second, power and coherence thresholding is applied to eliminate noisy sections. Third, a robust, least-squares technique is used to obtain the impedances. Fourth, the confidence intervals are calculated using the nonparametric jackknife method.

Processing of data begins with the transform of the EM time series into the wavelet domain. The data sets that we use in this example have 262,144 points and were acquired using a sampling rate of 40,690 Hz. To avoid rejecting segments because of the COI, we have not split the time series into short segments, and thus, only a few data points at the beginning and end are affected. This operation usually takes ~1 minute of computer time in a normal Pentium PC for six electromagnetic channels (four locals and two remotes). At the same time, deconvolution of the instrument response is applied also; and scales are converted to frequencies.

The second step consists of filtering data points using coherence and wavelet coherence thresholding techniques. The amount of data that are eliminated depends on the values of thresholding limits set by the user and the quality of the data. Figures 5–10 show the MT responses of sites analyzed in this study and a plot of percentage of data left after two-stage coherence thresholding. This later procedure eliminates, in most cases, more than 90% of the data. For longer periods, we have found that the coherence thresholding is not as efficient as in the AMT dead band, and we usually relax this thresholding; thus, the amount of data eliminated is smaller. The data that are not eliminated by coherence thresholding are used in the impedance tensor estimates of final responses using the IWLS technique described previously.

On the left panels of Figures 5 through 10 are the responses obtained from the code developed in this work; on the right are the responses obtained using a robust Fourier transform algorithm (bounded influence, remote reference processing, [BIRRP], Chave and Thomson, 2004), which represent the best conventional MT responses that we could obtain. The Fourier responses show scatter at all frequencies, especially in the AMT

dead band; whereas for the wavelet responses, the scatter is reduced to a few frequencies in the dead band.

As mentioned earlier, the nature of EM induction in the earth results in MT responses that must be smoothly varying with frequency. Therefore, we can consider the responses obtained with the new wavelet-processing scheme superior to those obtained with a Fourier method. The jackknifed confidence levels also are larger in the AMT dead band, suggesting either larger variability or few segments being used in the final calculation of MT responses.

The responses from sites 001, 005, and 006 show some important scatter at the AMT dead band. A method for analyzing this lack of reliable responses in this band, for these sites, is to calculate the global wavelet (equation 11) and its standard deviation to show the variability of spectra at each frequency. Figure 11 shows the global wavelet spectra for site 006 (continuous line) and the upper and lower limits of the standard deviation (dashed lines). This plot shows that signal levels of the magnetic fields (top figure) are very small in the AMT dead band and that there is very little variability in this band. This results from the lack of sufficient signal energy in this band, causing the magnetometer to record only noise. The processing method breaks down because it cannot find any suitable magnetic spectra in the AMT dead band.

For the electric channel (bottom figure), the situation is not as severe. This is normal behavior and the basis for development of the TTMT method by Garcia and Jones (2005). This plot shows that even when a transient is localized, the magnetic signal that it carries might not be measurable in the AMT dead band. At the same time, and because signal levels are so low, this demonstrates that, when processing data in the AMT dead band, it is important to eliminate noise in the electric field, rather than the magnetic field, and to accurately select the best segments.

These data were collected in July, in the middle of the Northern Hemisphere summer, which is statistically an ideal time for undertaking AMT measurements (Garcia and Jones, 2002). However, there is also strong daily variation from atmospheric ionization in the daytime, resulting in increased atmospheric conductivity and energy attenuation that causes the lack of signal during daytime.

The new results are superior to the ones obtained previously with BIRRP and the TTMT method, although the new algorithm uses the same techniques to solve the robust least-squares method and obtain final responses. Use of the CWT and the coherence threshold seem to be fundamental to improving responses in the AMT dead band.

Our code is designed for processing high-frequency data in the AMT band, but we have tested the present algorithm with longer period data. The results are not as satisfactory, and BIRRP and other processing codes usually give better results. For longer periods, the signal is not arriving in bursts of energy (transients); instead, bursts of higher amplitudes usually are caused by noise. Implementation of our approach for longer periods requires a redesign of the algorithm.

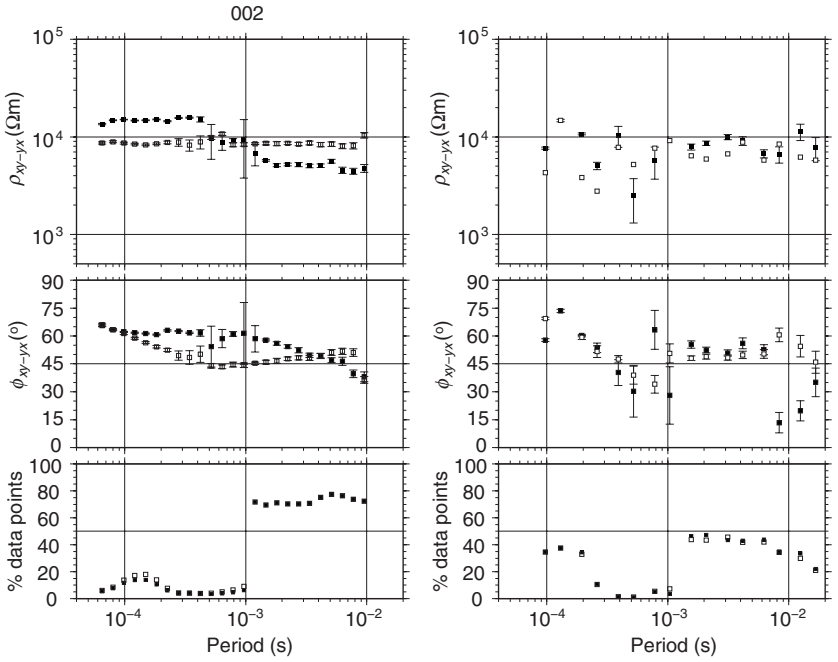

Figure 6. Same as Figure 5 at site 002.

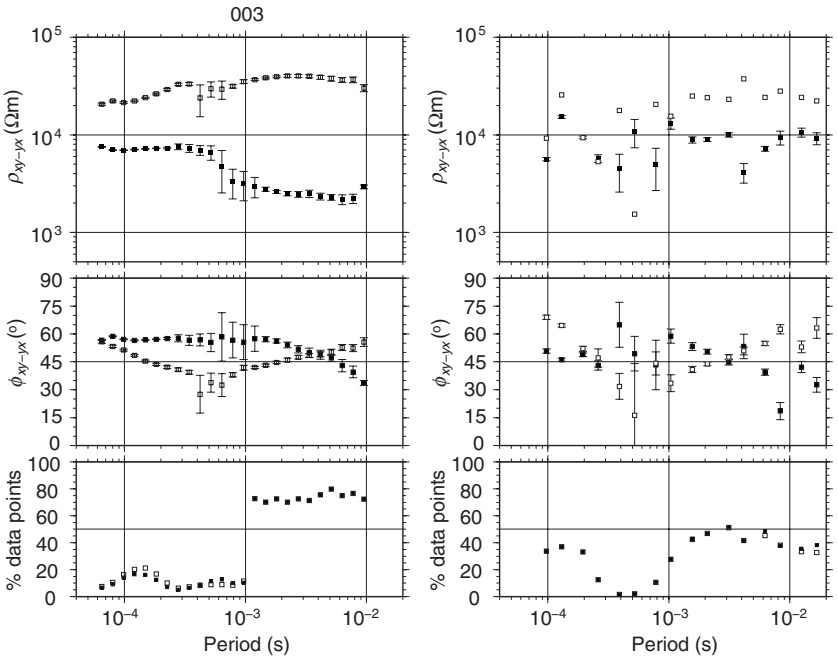

Figure 7. Same as Figure 5 at site 003.

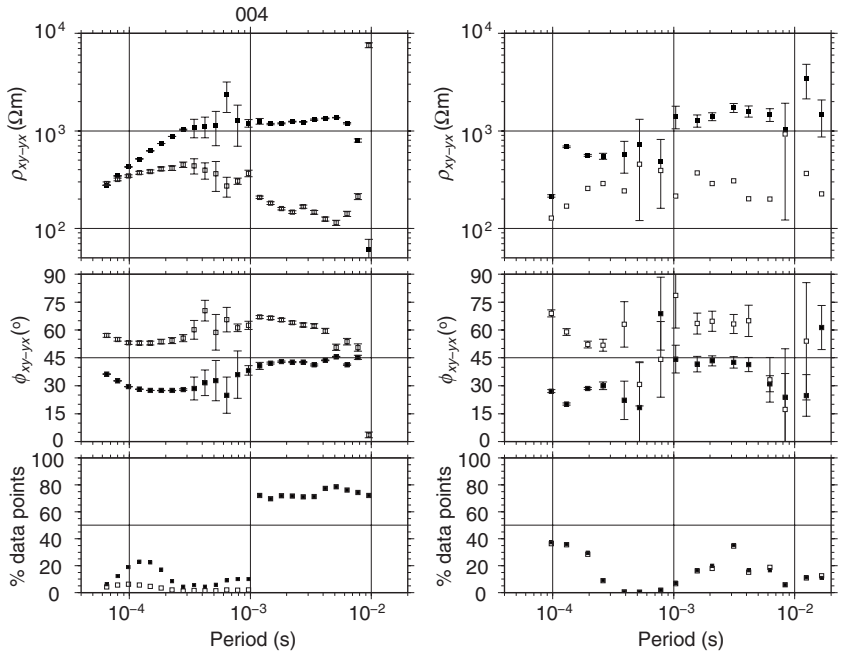

Figure 8. Same as Figure 5 at site 004.

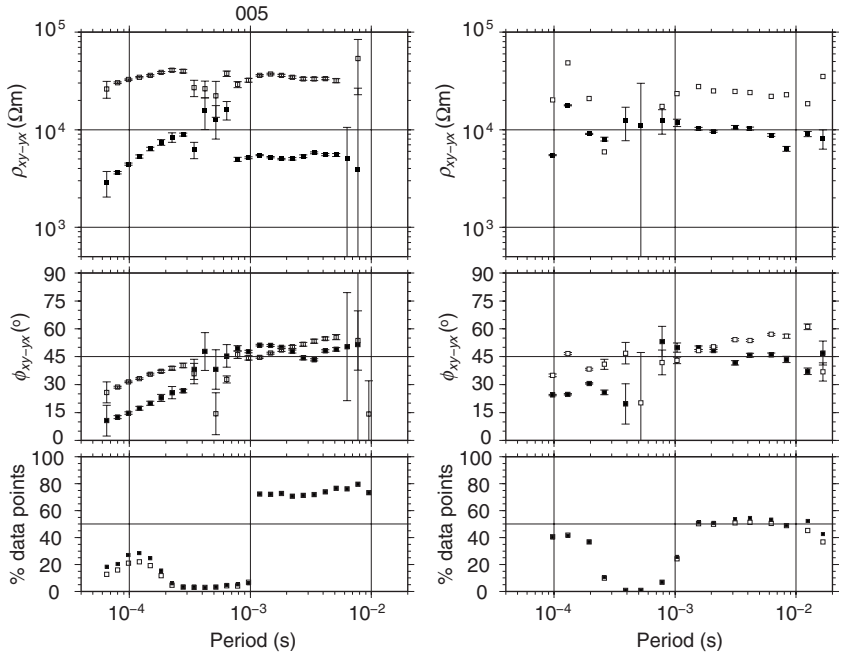

Figure 9. Same as Figure 5 at site 005.

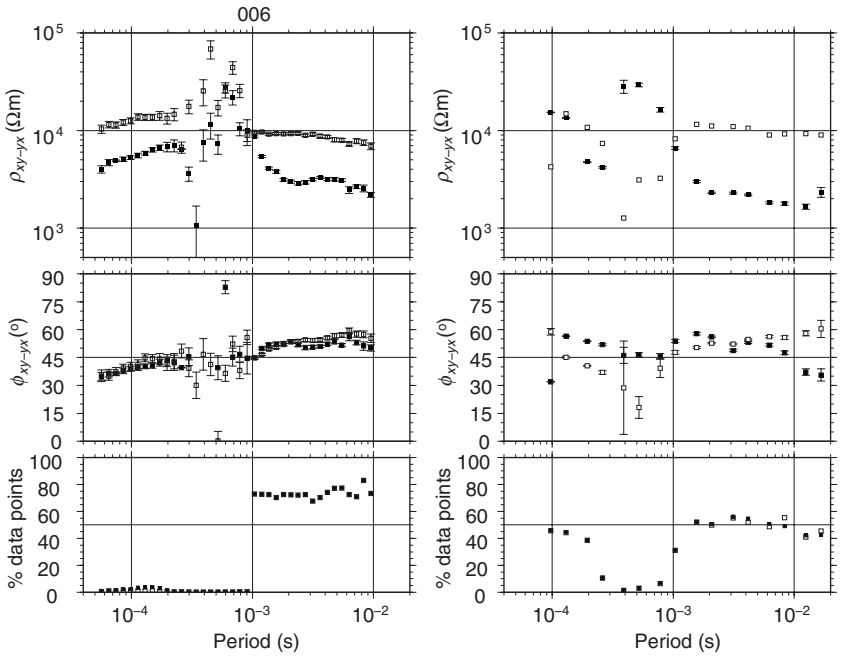

Figure 10. Same as Figure 5 at site 006.

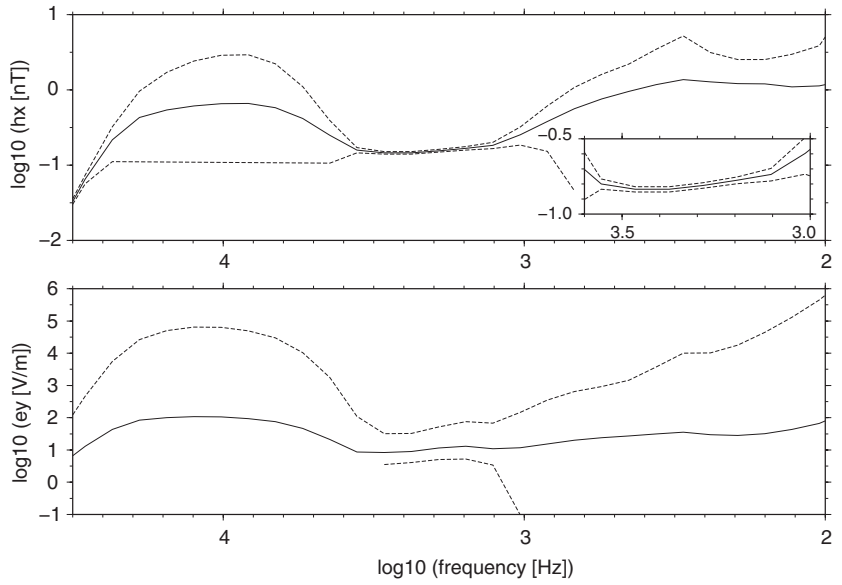

Figure 11. Global wavelet spectra (solid line) for the time series at site 006. The dashed lines show the standard deviation of these spectra. In the dead band, variability is small and can explain the poor results from the processing. The inset plot in the top panel is a zoom around the dead band.

CONCLUSIONS

We developed an algorithm to perform the continuous wavelet transform, using Morlet wavelets, of high-frequency audiomagnetotelluric (AMT) data, focusing on obtaining superior estimates in the AMT dead band of 1 kHz through 5 kHz. After wavelet estimation of spectra, initial selection of "good" segments is performed using classical and wavelet coherence thresholding. The algorithm uses a robust iterative solver to obtain reliable responses, and the confidence levels are calculated using a nonparametric jackknife technique.

AMT data from northern Ontario were used to test the code. These data were processed previously using a Fourier transform technique and a recent telluric-telluric magnetotelluric (TTMT) technique. Estimates obtained using the new algorithm are a significant improvement over previous results, and their quality (low scatter, small-error estimates) allow for their quantitative interpretation. There are instances, as in certain times of day, for which the wavelet-processing algorithm could not provide reliable responses in the AMT dead band.

Calculating the spectral standard deviation for one of these sites, we demonstrate that the measured magnetic fields show very little variability in the dead band. This is not the same in the electric fields, which is consistent with our earlier results; and our suggestion that at AMT dead band frequencies, one will obtain more stable estimates using electric fields as the remote references rather than magnetic fields. Overall, we demonstrate that because of the lack of signal, it is very important to use robust techniques to avoid introducing spurious segments in the final calculation of the transfer functions.

This work also shows that the location and use of high-energy events (transients) are insufficient to ensure good-quality responses. The AMT data from northern Canada show in some instances a minimum of energy and a lack of variability, proving that even the few transients that arrive at the site location do not raise the energy level; and this effect is worse in sites occupied later in the afternoon (005 and 006).

ACKNOWLEDGMENTS

The authors thank INCO and Geosystem for providing the data. This work was initiated while Xavier Garcia was a visiting fellow at the Geological Survey of Canada (GSC), Ottawa; and the authors acknowledge the GSC, INCO, Phoenix Geophysics, and Geosystem for Xavier Garcia's funding. The authors thank the associate editor, Kerry Key, and three anonymous reviewers for their comments. P. Wessel and W. H. F. Smith developed the GMT plotting package used by the authors to make plots.

REFERENCES

Akaike, H., 1967, Some problems in the application of the cross-spectral method, *in* B. Harris, ed., Advanced seminar on spectral analysis of time series: John Wiley and Sons, 81–107.

Bendat, J. S., and A. G. Piersol, 1971, Random data: Analysis and measurement procedures: John Wiley and Sons.

Box, G. E. P., 1953, Non-normality and tests on variance: Biometrika, **40**, 318–335.

Chave, A. D., and A. G. Jones, 1997, Electric and magnetic field galvanic distortion decomposition of BC87 data: Journal of Geomagnetism and Geo-

electricity, **49**, 4669–4682.
Chave, A. D., and D. J. Thomson, 1989, Some comments on magnetotelluric response function estimation: Journal of Geophysical Research, **94**, 14215–14225.
———, 2003, A bounded influence regression estimator based on the statistics of the hat matrix: Journal of the Royal Statistical Society, Series C (Applied Statistics), **52**, 307–322.
———, 2004, Bounded influence estimation of magnetotelluric response functions: Geophysical Journal International, **157**, 988–1006.
Chave, A. D., D. J. Thomson, and M. E. Ander, 1987, On the robust estimation of power spectra, coherences, and transfer functions: Journal of Geophysical Research, **92**, 633–648.
Daubechies, I., 1990, The wavelet transform, time-frequency localization and signal analysis: IEEE Transactions on Information Theory, **36**, 961–1005.
Dmitriev, V. I., and M. N. Berdichevsky, 1979, The fundamental model of magnetotelluric sounding: Proceedings of the IEEE, **67**, 1033–1044.
Efron, B., 1982, The jackknife, the bootstrap, and other resampling plans: SIAM.
Egbert, G. D., and J. Booker, 1986, Robust estimation of geomagnetic transfer functions: Geophysical Journal of the Royal Astronomical Society, **87**, 173–194.
Egbert, G. D., and D. Livelybrooks, 1996, Single station magnetotelluric impedance estimation: Coherence weighting and the regression M-estimate: Geophysics, **61**, 964–970.
Farge, M., 1992, Wavelet transforms and their applications to turbulence: Annual Review of Fluid Mechanics, **24**, 395–457.
Foufoula-Georgiou, E., and P. Kumar, 1995, Wavelets in geophysics: Academic Press.
Gamble, T. D., W. M. Goubau, and J. Clarke, 1979, Magnetotellurics with a remote reference: Geophysics, **61**, 53–68.
Garcia, X., and A. G. Jones, 2002, Atmospheric sources for audio-magnetotelluric (AMT) sounding: Geophysics, **67**, 448–458.
———, 2005, New methodology for the acquisition and processing of audio-magnetotelluric (AMT) data in the dead-band: Geophysics, **70**, 119–126.
Geary, R., 1943, Relations between statistics: The general and the sampling problem when the samples are large: Proceedings of the Royal Irish Academy, **49**, 177–196.
Gini, C., 1921, Sullâ interpolazione di una retta quando i valori della variabile indipendente sono affetti da errori accidentali: Metron, **1**, 63–82.
Goupillaud, P., A. Grossmann, and J. Morlet, 1984, Cycle-octave and related transform in seismic signal analysis: Geoexploration, **33**, 85–102.
Grossman, A., and J. Morlet, 1987, Decomposition of hardy functions into square integrable wavelets of constant shape: SIAM Journal of Mathematical Analysis, **15**, 723–736.
Hinkley, D. V., 1977, Jackknifing in unbalanced situations: Technometrics, **19**, 285–292.
Huber, P., 1964, Robust estimation of a location parameter: Annals of Mathematical Statistics, **35**, 73–101.
Jones, A. G., A. D. Chave, G. Egbert, D. Auld, and K. Bahr, 1989, A comparison of techniques for magnetotelluric response function estimation: Journal of Geophysical Research, **94**, 14201–14213.
Jones, A. G., and H. Joedicke, 1984, Magnetotelluric transfer function estimation improvement by a coherence-based rejection technique: 56th Annual International Meeting, SEG, Expanded Abstracts, 51–55.
Kaiser, G., 1994, A friendly guide to wavelets: Birkhäuser.
Larsen, J. C., 1989, Transfer functions: Smooth robust estimates by least squares and remote reference methods: Geophysical Journal International, **99**, 655–663.
Mallat, S., 1998, A wavelet tour of signal processing: Academic Press.
McNeice, G. W., and A. G. Jones, 2001, Multisite, multifrequency tensor decomposition of magnetotelluric data: Geophysics, **66**, 158–173.
Meyers, S. D., B. G. Kelly, and J. J. O'Brien, 1993, An introduction to wavelet analysis in oceanography and meteorology: With application to the dispersion of Yanai waves: Monthly Weather Review, **121**, 2858–2866.
Percival, D. B., 1995, On estimation of the wavelet variance: Biometrika, **82**, 619–631.
Percival, D. B., and A. T. Walden, 2000, Wavelet methods for time series analysis: Cambridge University Press.
Reiersøl, O., 1941, Confluence analysis by means of lag moments and other methods of confluence analysis: Econometrica, **9**, 1–22.
———, 1950, Identifiability of a linear relation between variables which are subject to error: Econometrica, **18**, 375–389.
Schultz, A., R. D. Kurtz, A. D. Chave, and A. G. Jones, 1993, Conductivity discontinuities in the upper mantle beneath a stable craton: Geophysical Research Letters, **20**, 2941–2944.
Sims, W. E., F. X. Bostick, and H. W. Smith, 1971, The estimation of magnetotelluric impedance tensor elements from measured data: Geophysics, **36**, 938–942.
Smirnov, M., 2003, Magnetotelluric data processing with a robust statistical procedure having a high breakdown point: Geophysical Journal International, **152**, 1–7.
Thomson, D. J., and A. D. Chave, 1991, Jackknifed error estimates for spectra, coherences, and transfer functions, *in* S. Haykin, ed., Advances in spectrum analysis and array processing, v. 1: Prentice Hall, 58–113.
Thomson, L. W., 1860, Electricity atmospheric: Nichols Cyclopedia.
Torrence, C., and G. P. Compo, 1998, A practical guide to wavelet analysis: Bulletin of the American Meteorological Society, **79**, 61–78.
Torrence, C., and P. Webster, 1999, Interdecadal changes in the ENSO-monsoon system: Journal of Climate, **12**, 2679–2690.
Trad, D. O., and J. M. Travassos, 2000, Wavelet filtering of magnetotelluric data: Geophysics, **65**, 482–491.
Weng, H., and K. M. Lau, 1994, Wavelets, period doubling, and time-frequency localization with application to organization of convection over the tropical Western Pacific: Journal of Atmospheric Science, **51**, 2523–2541.
Wilson, C. T. R., 1920, Investigation on lightning discharges and on the electric field of thunderstorms: Phylosophical Transactions of the Royal Society of London, Series A, 221, 73–115.
Zhang, Y., D. Goldak, and K. Paulson, 1997, Detection and processing of lightning-sourced magnetotelluric transients with the wavelet transform: IEICE Transactions on Fundamentals of Electronics, Communications and Computer Sciences, **E80**, 849–858.
Zhang, Y., and K. V. Paulson, 1997, Enhancement of signal-to-noise ratio in natural-source transient MT data with wavelet transform: Pure and Applied Geophysics, **149**, 405–419.